Analysis of next- and third-generation RNA-Seq data reveals the structures of alternative transcription units in bacterial genomes

Qi Wang[1], Zhaoqian Liu[1,2], Bo Yan[3], Wen-Chi Chou[4], Laurence Ettwiller[3], Qin Ma[2,†], and Bingqiang Liu[1,†]

[1] School of Mathematics, Shandong University, Jinan 250200, China.

[2] Department of Biomedical Informatics, College of Medicine, The Ohio State University, Columbus, OH 43210, USA.

[3] New England Biolabs Inc., Ipswich, MA 01938, USA.

[4] Infectious Disease and Microbiome Program, Broad Institute of MIT and Harvard, Cambridge, MA 02142, USA.

†Corresponding author. Email: bingqiang@sdu.edu.cn (B.L.); qin.ma@osumc.edu (Q.M.)

ABSTRACT

Alternative transcription units (ATUs) are dynamically encoded under different conditions or environmental stimuli in bacterial genomes, and genome-scale identification of ATUs is essential for studying the emergence of human diseases caused by bacterial organisms. However, it is unrealistic to identify all ATUs using experimental techniques, due to the complexity and dynamic nature of ATUs. Here we present the first-of-its-kind computational framework, named SeqATU, for genome-scale ATU prediction based on next-generation RNA-Seq data. The framework utilizes a convex quadratic

programming model to seek an optimum expression combination of all of the to-be-identified ATUs. The predicted ATUs in *E. coli* reached a precision of 0.77/0.74 and a recall of 0.75/0.76 in the two RNA-Sequencing datasets compared with the benchmarked ATUs from third-generation RNA-Seq data. We believe that the ATUs identified by SeqATU can provide fundamental knowledge to guide the reconstruction of transcriptional regulatory networks in bacterial genomes.

INTRODUCTION

An operon in bacterial genomes is defined as a group of consecutive genes regulated by a common promoter that all share the same terminator (*1*). Genes in the same operon generally encode proteins with relevant or similar biological functions; e.g., *lacZ*, *lacY*, and *lacA* in the *lac* operon encode proteins that help cells use lactose (*1, 2*). With decades of research on bacterial transcriptional regulation, the operon model has been found to have complex mechanisms that control expression (*3*-*5*). Multiple studies have shown that bacterial genes are dynamically transcribed under different triggering conditions, leading to shared genes among different mRNA transcripts (*6*-*8*). This dynamic architecture can be redefined by all of the alternative transcription units (a.k.a., ATUs) (*3, 5*), and more details can be found in fig. S1.

ATU identification is of fundamental importance for understanding the transcriptional regulatory mechanisms of bacteria, and these dynamic structures have been demonstrated to be associated with human diseases (*9*-*12*). For example, Bhat *et al*. studied the *alr-groEL1* operon, which is essential for the survival or virulence of *M. tuberculosis* (*9, 11*), the causative agent of tuberculosis (TB), and found that

the regulation of the sub-operon is distinct from the main operon (*alr-groEL1* operon) under stress, especially during heat shock, pH, and SDS stresses (*9*). Another example is *Helicobacter pylori*, a gastric pathogen that is the primary known risk factor for gastric cancer (*12*). Sharma *et al*. found an acid-induced sub-operon *cag*22-18 transcribed from the primary *cag*25-18 operon in the *cag* pathogenicity island of the *H. pylori* genome under acid stress (*10*). The mechanism of the complex ATU structure in these pathogenic bacteria can help us to study the emergence of human diseases caused by bacterial organisms.

Several newly developed techniques have provided a comprehensive view of the *E. coli* transcriptome by identifying full-length primary transcripts (*13-17*). For example, SMRT-Cappable-seq (*6*) combines the isolation of the full-length bacterial primary transcriptome with PacBio SMRT (Single Molecule, Real-Time) sequencing (*6*), and simultaneous 5' and 3' end sequencing (SEnd-seq) (*7*) captures both transcription start sites (TSSs) and transcription termination sites (TTSs) via circularization of transcripts (*17*). Despite the great progress in experimental techniques, there are still some deficiencies. On the one hand, the read depth and error rate of the third-generation sequencing used in SMRT-Cappable-seq have an impact on ATU prediction compared with Illumina-based RNA-Seq (*7, 18*). On the other hand, the time-consuming, laborious, and costly properties of these experimental techniques make them unrealistic to be generally applicable to ATU predictions in bacteria under specific conditions. Thus, novel and robust computational methods for ATU identification in bacterial genomes based on RNA-Seq are urgently needed.

Fortunately, many computational studies have been carried out to predict ATUs in bacteria, which have provided some preliminary studies for ATU prediction. Several public databases, such as RegulonDB (*19*), DBTBS(*20*), MicrobesOnline (*21*), DOOR (*22, 23*), OperomeDB (*24*), DMINDA 2.0 (*25*), and ProOpDB (*26*), provide various levels of operon information and small amounts of ATU information. However, these databases cannot provide genome-scale ATU information under specific conditions. Some computational studies, including Rockhopper (*27*), SeqTU (*4, 28*), BAC-BROWSER(*29*), rSeqTU (*5*), and Operon-mapper (*30*), utilize machine learning and model integration methods based on genomic information and gene expression profiles to identify bacterial transcription architecture. However, these works still cannot solve the dynamic patterns and overlapping nature of ATUs.

Here, we present SeqATU, a novel computational method for genome-scale ATU prediction by analyzing next- and third-generation RNA-Seq data (Fig. 1 and table S1). SeqATU utilizes a convex quadratic programming model (CQP) and aims to provide the optimum expression combination of all of the to-be-identified ATUs. Specifically, CQP minimizes the squared error between the predicted expression level of ATUs and the actual expression levels in genetic and intergenic regions. It is noteworthy that SeqATU also utilizes the information about the bias rate function in modeling non-uniform read distribution as the linear constraints of CQP to profile the complexity of the ATU architecture. Overall, SeqATU provides a generalized framework for the inference of ATUs based on next-generation RNA-Seq data collected under multiple conditions and can be easily applied to any

bacterial organism to identify the ATU architecture and construct a transcriptional regulatory network.

Please place Fig. 1 here.

MATERIALS AND METHODS

Data collection

The two Cappable RNA-Seq datasets used in this study, M9Enrich_Seq and RiEnrich_Seq, were obtained from *E. coli* grown under two different conditions: M9 minimal medium and Rich medium, respectively (6). The full-length primary transcripts were enriched as described in (6) with modifications to be adapted to Illumina sequencing. The capping and polyA tailing were performed as described in (6). The capped RNA was enriched using hydrophilic streptavidin magnetic beads (New England Biolabs) and eluted with Biotin using the same condition (6). Differently, the eluted RNA was enriched once more using streptavidin beads to further remove processed RNA (e.g., rRNA). Subsequently, the eluted RNA was used for library preparation using NEBNext Ultra II directional RNA library prep kit (E7760). Sequencing was performed on the Illumina Miseq system (paired-end, 100bp). All reads were mapped to the *E. coli* genome using Burrows-Wheeler Aligner (BWA) with the default parameters (*31*). Read alignment and other computational analyses were carried out using the *E. coli* genome NC_000913.3, and the corresponding gene annotations (GCF_000005845.2_ASM584v2_genomic.gff) were downloaded from NCBI. Two experimentally verified ATU datasets, SMRT_M9Enrich and SMRT_RiEnrich, were used as the benchmark data to evaluate the predicted ATUs, which were

generated by SMRT-Cappable-seq under the same conditions as the Illumina datasets M9Enrich_Seq and RiEnrich_Seq, respectively (*6*). In addition, the ATUs defined by RegulonDB (*19*) and SEnd-seq (*7*) were also used as additional evaluation data in our study.

Calculation of the expression values of genetic and intergenic regions

After the RNA-Seq reads in M9Enrich_Seq and RiEnrich_Seq were mapped to the *E. coli* genome using BWA, we determined the number of reads $N(l)$ covering each genomic position l. Suppose that g_{i} and $g_{\mathrm{i+1}}$ are two consecutive genes on the same strand; we denote the expression value of g_i as c_i and the expression value of the intergenic region between genes g_i and g_{i+1} as $b_{i,i+1}$. Then, the calculation of c_i and $b_{i,i+1}$ is given by:

$$c_i = \frac{\sum_{k \in g_i} N(k)}{|g_i|} \tag{1}$$

$$b_{i,i+1} = \frac{\sum_{l \in g_{i,i+1}} N(l)}{|g_{i,i+1}|} \tag{2}$$

where $k \in g_i$ denotes that genomic position k is on the gene g_i and $|g_i|$ denotes the genomic length of g_i.

Modeling non-uniform read distribution along mRNA transcripts

We introduced the bias rate function, which is similar to the bias curves in the work of Wu *et al*. (*32*), to address the non-uniform distribution of the RNA-Seq reads along mRNA transcripts (*32-35*). The bias function reflects the relative read distribution bias from the 3' end to the 5' end of an mRNA transcript.

We assumed that the maximum read coverage of all the genomic positions of an mRNA transcript is the expression level without bias. It is noteworthy that a single gene mRNA transcript with no shared gene among different mRNA transcripts can serve as the ideal template for modeling non-uniform read distribution along mRNA transcripts. The specific steps of modeling non-uniform read distribution are detailed as follows:

Step 1: Single Gene mRNA Transcript Selection. We selected single gene mRNA transcripts from the evaluation data and plotted their expression distributions. Specifically, 12 groups of single gene mRNA transcripts with lengths ranging from 300 to 1,500 bp were selected from the evaluation data (more details are given in method S1), and each group had ten randomly chosen mRNA transcripts. Apparent decline trends appeared in the single gene mRNA transcripts with long lengths, ranging from 1,100 to 1,500 bp (fig. S2). The reason for this phenomenon may be that the incomplete transcription and 3' end degradation or processing induce the enrichment of signal at 5' end of the mRNA transcripts with long lengths (*36, 37*). Finally, we plotted the expression distribution of single gene mRNA transcripts with lengths ranging from 1,100 to 1,500 bp.

Step 2: Acquiring the Bias Rate Function. We applied nonlinear regression to the expression distribution of the selected single gene mRNA transcripts and acquired the hypothetical function $f(x)$. Specifically, the x axis and y axis of the expression distribution were converted to the distance from the 3' end of an mRNA transcript and the bias rate of read distribution, respectively. To apply nonlinear regression to single gene mRNA transcripts with different lengths, normalization was also implemented

on x. Here, $x = (x_1, x_2, \dots, x_m)$ and $y = (y_1, y_2, \dots, y_m)$ are defined by:

$$x_i = \begin{cases} \frac{l_m - l_{m-i+1}}{max_l - l_1} \times 10^3, & forward \\ \frac{l_i - l_1}{max_l - l_1} \times 10^3, & reverse \end{cases} \quad (3)$$

$$y_i = \begin{cases} \frac{N(l_{m-i+1})}{max_y}, & forward \\ \frac{N(l_i)}{max_y}, & reverse \end{cases} \quad (4)$$

where m denotes the number of genomic positions on an mRNA transcript; $l = (l_1, l_2, \dots, l_m)$ denotes the genomic positions on an mRNA transcript; $max_l = l_m$; $N(l_i)$ denotes the expression level of the genomic position l_i, i.e., the number of reads covering the genomic position l_i; and max_y denotes the expression level without bias in an mRNA transcript, which is calculated as $max\{N(l_i)\}$, $1 \le i \le m$. We used the function *nls* in R to acquire the hypothetical function $f(x)$.

Step 3: Constructing Bias Rate Vectors. We constructed a genetic or intergenic region bias rate vector for each mRNA transcript by calculating the bias rate of all of its component genetic or intergenic regions. The bias rate of a genetic or an intergenic region is the average bias rate of all the genomic positions that it contains. Considering an mRNA transcript T and its component gene set $\{g_1, g_2, \dots, g_n\}$ (the details of the gene labels are described in method S2), we denoted the genetic region bias rate vector as $\boldsymbol{u} = (u_1, u_2, \dots, u_n)$, which was calculated using the formula:

$$u_i = \begin{cases} \frac{\sum_{t=m-i_q+1}^{m-i_p+1} f(x_t)}{x_{m-i_p+1} - x_{m-i_q+1} + 1}, & forward \\ \frac{\sum_{t=i_p}^{i_q} f(x_t)}{x_{i_q} - x_{i_p} + 1}, & reverse \end{cases} \quad (5)$$

where m denotes the number of genomic positions on T; u_i denotes the bias rate of g_i for T; and $L_g = (l_{1_p}, l_{1_q}, l_{2_p}, l_{2_q}, \ldots, l_{n_p}, l_{n_q})$ is the range of the genomic positions of $\{g_1, g_2, \ldots, g_n\}$, while the range of the genomic positions of g_i is $[l_{i_p}, l_{i_q}]$, $1 \leq i \leq n$. Similarly, the calculation of the intergenic region bias rate vector $\boldsymbol{v} = (v_1, v_2, \ldots, v_{n-1})$ is provided in method S3.

Modification of maximal ATU clusters

A maximal ATU cluster is defined as a maximal consecutive gene set such that each pair of its consecutive genes can be covered by at least one ATU. Similar to ATUs, maximal ATU clusters are also dynamically composed under different conditions or environmental stimuli in bacterial genomes (*5, 38*). Such a maximal ATU cluster can be used as an independent genomic region for ATU prediction, which alleviates the difficulty in computationally predicting ATUs at the genome scale. The output of our in-house tool rSeqTU can serve as the maximal ATU cluster data, which lays a solid foundation for ATU prediction (*5*). We modified the maximal ATU clusters from rSeqTU: (*i*) two maximal ATU clusters with distances less than 40 bp were combined into one cluster and (*ii*) a maximal ATU cluster was split at the intergenic region where the opposite-strand genes were located. In addition, we selected the maximal ATU clusters with expression values over ten (see the details in method S4), according to the study of Etwiller *et al*. (*13*).

The mathematical programming model for ATU prediction

The predicted ATU expression profile should be consistent with the observed expression profiles of the

158 genetic and intergenic regions. Therefore, the prediction of the ATU profiles can be modeled as an
159 optimization problem, which seeks an optimum expression combination of all of the to-be-identified
160 ATUs to minimize the gap between the predicted ATUs and the observed genetic and intergenic region
161 expression profiles. Here, a convex quadratic programming model was built to solve this optimization
162 problem.

163 We denoted a maximal ATU cluster as G, assuming that it contains the consecutive genes
164 $\{g_1, \dots, g_n\}$, and the intergenic regions of these genes are $\{g_{1,2}, \dots, g_{n-1,n}\}$. The size of G is defined as
165 the number of its component genes n. Theoretically, there are $\frac{n\times(n+1)}{2}$ ATUs for G, and an ATU with
166 consecutive genes $\{g_i, g_{i+1}, \dots, g_j\}$ is denoted as $a^{i,j}$; the corresponding expression value is $x^{i,j}$, $1 \leq$
167 $i \leq j \leq n$.

168 For the component gene g_k of G, the gap between the gene expression value c_k and the sum of the
169 expression level of the ATUs containing it is denoted as τ_k, which provides the first n equality
170 constraints in our mathematical programming model, $k = 1,2, \dots, n$. Similarly, for the intergenic region
171 $g_{l,l+1}$ of G, the gap between the intergenic region expression value $b_{l,l+1}$ and the sum of the
172 expression level of the ATUs containing it is denoted as β_l, providing the last $n-1$ equality
173 constraints in our mathematical programming model, $l = 1,2, \dots, n-1$.

174 The goal of our mathematical programming model is to minimize the square of $\boldsymbol{\varepsilon} =$
175 $(\tau_1, \tau_2, \dots, \tau_n, \beta_1, \dots, \beta_{n-1})$, as the combination of $x^{i,j}$ with a minimal value of $\boldsymbol{\varepsilon}\boldsymbol{\varepsilon}^T$ is corresponding to
176 an optimum expression combination of all ATUs $a^{i,j}$ for G, $1 \leq i \leq j \leq n$. Additionally, to control the

number of optimal solutions and reduce the false-positive errors, we added an L^1 regularization $\alpha||\boldsymbol{x}||_1$ to $\boldsymbol{\varepsilon}\boldsymbol{\varepsilon}^T$ with $x^{i,j} \geq 0$, which is a linear function. Because of the variant expression level of different maximal ATU clusters, we used the expression value of G as α. In total, the convex quadratic programming model with unknown variables $(\boldsymbol{x}, \boldsymbol{\varepsilon})$ is shown as follows:

$$
\begin{aligned}
&min && \boldsymbol{\varepsilon}\boldsymbol{\varepsilon}^T + \alpha||\boldsymbol{x}||_1 && \\
&s.t. && \sum_{i=1}^{k}\sum_{j=k}^{n} u_{i,k}x^{i,j} = c_k + \tau_k && k = 1,2,\dots,n \\
& && \sum_{i=1}^{l}\sum_{j=l+1}^{n} v_{i,l+1}x^{i,j} = b_{l,l+1} + \beta_l && l = 1,2,\dots,n-1 \\
& && \boldsymbol{x} = \left(x^{i,j}\right), \quad x^{i,j} \geq 0 && 1 \leq i \leq j \leq n \\
& && \boldsymbol{\varepsilon} = (\tau_1, \tau_2, \dots, \tau_n, \beta_1, \dots, \beta_{n-1}) && (6)
\end{aligned}
$$

where $\boldsymbol{u} = (u_{i,j})$ is the genetic region bias rate vector for G, $u_{i,j}$ is the bias rate of gene g_j for ATU $a^{i,k}$, $1 \leq i \leq j \leq n$, $j \leq k \leq n$, $\boldsymbol{v} = (v_{p,q})$ is the intergenic region bias rate vector for G, and $v_{p,q}$ is the bias rate of the intergenic region $g_{q-1,q}$ for ATU $a^{p,l}$, $1 \leq p < q \leq n$, $q \leq l \leq n$ (see the details in method S5).

Two evaluation methods for ATU prediction

In the first evaluation method, precision and recall were defined based on perfect matching (Eqs. 7). Perfect matching of two ATUs means that all of their component genes are the same. Here, the true positives (TP) are the number of predicted ATUs with the same component genes as an ATU in the evaluation data; the false positives (FP) are the number of predicted ATUs that do not exist in the

evaluation data; the false negatives (FN) are the number of ATUs that appear in the evaluation data but not in the prediction results of SeqATU.

$$precision = \frac{TP}{TP + FP}$$
$$recall = \frac{TP}{TP + FN} \quad (7)$$

In the second evaluation method, precision and recall were defined based on relaxed matching, which is measured by the similarity of two ATUs. Assuming that an ATU t is in one of two datasets (the predicted ATU dataset and evaluated ATU dataset), the definition and calculation of the similarity of t are shown in the following three cases:

Case 1: If t shares boundary genes at both ends of an ATU in the other dataset, i.e., all component genes of t are the same as one in the other dataset, then $similarity(t) = 1$.

Case 2: If t shares exactly one boundary gene of ATUs in the other dataset, then we denote U_a as the ATUs in the other dataset that share the 5'-end gene with t and denoted U_b as the ATUs in the other dataset that share the 3'-end gene with t, $U_a \cap U_b = \emptyset$, one of U_a and U_b can be empty. Then,

$$similarity(t) = \frac{1}{2} max_{t' \in U_a} \frac{\alpha(t')}{\beta(t')} + \frac{1}{2} max_{t' \in U_b} \frac{\alpha(t')}{\beta(t')} \quad (8)$$

where $\alpha(t')$ is the number of shared genes of t and t' and $\beta(t')$ is the maximal size of t and t'.

Case 3: If t shares no boundary genes at both ends of the ATUs in the other dataset, then $similarity(t) = 0$.

Finally, the precision and recall based on relaxed matching are calculated by the following formula:

$$precision = \frac{\sum_{t \in T_1} similarity(t)}{n_1}$$

$$recall = \frac{\sum_{t \in T_2} similarity(t)}{n_2} \quad (9)$$

where T_1 is the set of predicted ATUs, n_1 is the number of predicted ATUs, T_2 is the set of evaluated ATUs, and n_2 is the number of evaluated ATUs.

RESULTS

A reliable bias rate function is acquired in modeling non-uniform read distribution along mRNA transcripts

To ensure the reliability of the bias rate function in modeling non-uniform read distribution, we selected four single gene mRNA transcript datasets randomly from the two evaluation datasets (SMRT_M9Enrich and SMRT_RiEnrich), named M9Enrich_1, M9Enrich_2, RiEnrich_1, and RiEnrich_2. Four bias rate functions, which are exponential functions, were generated after conducting nonlinear regression on the mRNA transcripts across these four datasets (Fig. 2). We found that these bias rate functions were similar ($R^2 > 0.998$) when we evaluated the R-square statistic (for more details, see method S6 and table S2). The similarity of the four bias rate functions indicated that the selection of the single gene mRNA transcript datasets had little impact on modeling non-uniform read distribution along mRNA transcripts, implying the universal common non-uniform read distribution of different mRNA transcripts of *E. coli*. Specifically, we used the average of these four coefficients as the final coefficients of the exponential function, which was $f(x) = ae^{bx}$ with $a = 0.256$ and $b = 0.00128$.

Please place Fig. 2 here.

ATUs predicted by SeqATU reach precision and recall over 0.64

The performance evaluation was conducted by comparing the predicted ATUs with the ATUs in SMRT_M9Enrich and SMRT_RiEnrich, which were generated based on the third-generation sequencing and are not sensitive to transcripts with low expression levels. For a more accurate and fair evaluation, maximal ATU clusters after pre-selection were retained in the subsequent evaluations (more details about the pre-selection of maximal ATU clusters can be seen in method S7 and fig. S3).

The precision and recall of the predicted ATUs were calculated for each maximal ATU cluster. By considering only perfect matching, the average precision and recall were 0.67 and 0.67 for M9Enirch_Seq and 0.64 and 0.68 for RiEnrich_Seq, respectively. When using relaxed matching, the average precision and recall increased to 0.77 and 0.75 for M9Enrich_Seq and 0.74 and 0.76 for RiEnrich_Seq, respectively. The statistics for precision and recall on maximal ATU clusters with different sizes, as shown in Fig. 3A and fig. S4A. These results showed that the average precision and recall were decreasing with the increasing size of maximal ATU clusters (other than several large size ones due to their small number of counts). The results also indicated that the evaluation results based on relaxed matching were significantly higher than those based on perfect matching across different sizes. This result implied that the incorrectly predicted ATUs by SeqATU based on perfect matching tended to have strong similarities with the ATUs in the evaluation data. In addition, we also found that more than a quarter of the incorrectly predicted ATUs (25%/29% for M9Enrich_Seq/RiEnrich_Seq) by SeqATU

based on perfect matching matched with the transcription units in RegulonDB (*19*).

The two evaluation datasets (SMRT_M9Enrich and SMRT_RiEnrich) were both from SMRT-Cappable-seq, while one of the processing steps of the technique filtered RNA reads smaller than 1,000 bp (*6*), which indicated that the ATUs in these two evaluation datasets were not comprehensive. To address this issue, we enriched the evaluation data by adding the ATUs defined by SEnd-seq (*7*), as SEnd-seq did not introduce any filtering based on RNA size. When we used the new evaluation data, the ATUs predicted by SeqATU improved by 15% (0.77) and 19% (0.76) in terms of the average precision based on perfect matching for M9Enrich_Seq and RiEnrich_Seq, respectively, and by 9% (0.84) and 12% (0.83) based on relaxed matching. The statistics for precision across different sizes of the maximal ATU clusters are shown in Fig. 3B and fig. S4B, showing that the values of precision based on perfect matching were significantly improved across different sizes of maximal ATU clusters by using the evaluated ATUs from SMRT-Cappable-seq and SEnd-seq. This result suggested that the ATUs we predicted, which were not in SMRT_M9Enrich and SMRT_RiEnrich, may be due to the RNA length selection of SMRT-Cappable-seq. We enriched the evaluation data by adding the ATUs in RegulonDB (*19*) and also found the improvement of precision across different sizes of maximal ATU clusters for M9Enrich_Seq and RiEnrich_Seq (fig. S4C).

Furthermore, to facilitate the understanding of the performance of SeqATU and to measure the influence of the maximal ATU clusters from rSeqTU on our ATU prediction method, SMRT maximal ATU clusters collected from SMRT_M9Enrich and SMRT_RiEnrich (for more details, see method S8)

were applied for the CQP in two conditions (M9 minimal medium and Rich medium). We found that precision and recall increased to 0.73 and 0.77 for M9Enrich_Seq, respectively, and 0.69 and 0.80 for RiEnrich_Seq based on perfect matching (fig. S4D). Additionally, when using relaxed matching, precision and recall significantly increased to 0.82 and 0.84 for M9Enrich_Seq, respectively, and 0.79 and 0.86 for RiEnrich_Seq (fig. S4D). The significantly improved results verified the ability of SeqATU to accurately predict ATU when giving more accurate maximal ATU clusters. In addition, we found that the number of predicted ATUs and the evaluated ATUs under the maximal ATU cluster with the same size were similar except for the maximal size (Fig. 3C), and they were far less than the theoretical number, which indicated that SeqATU can effectively exclude most of the incorrect ATUs.

Please place Fig. 3 here.

The bias rate constraints efficiently improve the ability of SeqATU to predict ATUs

We tried to use SeqATU without bias rate constraints to predict the ATUs of *E. coli* and found that its performance significantly decreased compared with SeqATU (Fig. 4 and fig. S5). Specifically, the F-score of SeqATU without bias rate constraints was 0.69/0.68 based on perfect matching for M9Enrich_Seq/RiEnrich_Seq, compared with 0.75/0.74 for SeqATU. When using relaxed matching, the F-score of SeqATU without bias rate constraints was 0.79/0.78 for M9Enrich_Seq/RiEnrich_Seq, compared with 0.83/0.83 for SeqATU. This result suggested that the bias rate constraints of SeqATU could capture useful information about the non-uniform distribution of the RNA-Seq reads along the

mRNA transcripts (*32-35*) and then efficiently improve the ability of the model to predict complex ATUs.

Please place Fig. 4 here.

ATUs predicted by SeqATU display a dynamic composition and overlapping nature

A total of 2,973 distinct ATUs were identified in M9 minimal medium, and 2,767 were identified in Rich medium. Among them, there were 1,423/1,550 distinct ATUs on the forward strand and 1,323/1,444 on the reverse strand for M9Enrich_Seq/RiEnrich_Seq. Each of the predicted ATUs was comprised of an average of 2.59 genes, with the largest ATU containing 28 genes across the two conditions. The distribution of the size of the predicted ATUs is shown in Fig. 5A, from which we can see that the majority of ATUs (more than 87%) contained fewer than five genes in M9 minimal medium and Rich medium. Approximately 41% of the genes in *E. coli* were contained in more than one ATU for M9Enrich_Seq, compared to 43% genes for RiEnrich_Seq, suggesting that the ATUs in a maximal ATU cluster generally overlapped with each other (Fig. 5B). In addition, there were 1,576 ATU maximal clusters for M9Enrich_Seq and 1,512 ATU maximal clusters for RiEnrich_Seq. SeqATU identified a total of 1,977 identical ATUs under the two conditions, whereas there were 1,786 distinct ATUs. Among the distinct ATUs across the two conditions, 394 ATUs were from the same maximal ATU clusters in the two maximal ATU cluster datasets, and the rest were from different maximal ATU clusters. The fact there were distinct ATUs under the two conditions suggests that ATUs are dynamically responsive to

296 different conditions or environmental stimuli (for more real examples about the ATUs under different
297 conditions, see fig. S6).

298 The dynamic composition of predicted ATUs by SeqATU is of great significance to understand the
299 interactions inside polymicrobial communities. For example, chronic airway infection by *Pseudomonas*
300 *aeruginosa* considerably contributes to lung tissue destruction and impairment of pulmonary function in
301 cystic-fibrosis (CF) patients (*39*). Marie *et al*. found that the presence of *E*. *coli* complemented the
302 growth defect of a *P*. *aeruginosa bioA*-disrupted mutant that is unable to grow on rich medium, and can
303 be beneficial to *P*. *aeruginosa* when biotin supply is limited (*39*). An ATU with a high expression level
304 coded by the *uvrB* gene is identified by SeqATU in Rich medium, while it does not exist in M9 minimal
305 medium (Fig. 6). We predicted the *uvrB* gene to be involved in the biotin metabolism pathway, as the
306 *bioB*, *bioF*, *bioC*, and *bioD* genes contained in a same ATU with it have been known in the biotin
307 metabolism KEGG pathway. Therefore, the observation by Marie *et al*. can be explained that the ATUs
308 coded by the *uvrB* gene of *E*. *coli* can provide the biotin supply for *P*. *aeruginosa* under rich medium.
309 This result showed that SeqATU could increase our understanding of interspecies competition and
310 cooperation, which play an important role in shaping the composition and structure of polymicrobial
311 bacterial populations.

312 Please place Fig. 5 here.

313 Please place Fig. 6 here.

Predicted ATUs by SeqATU are verified by experimental TSSs and TTSs

An experimental TSS dataset of *E. coli* from SEnd-seq (*7*) and a TF binding site dataset of *E. coli* from the experimental dataset of RegulonDB (*19*) were used to further verify the reliability of SeqATU and were named dataset 1 and dataset 2, respectively. There were 5,512 experimental TSSs in dataset 1 and 3,220 experimental TF binding sites in dataset 2. We considered the 5'-end genes and no 5'-end genes of the predicted ATUs by SeqATU. A gene that is not the 5'-end gene of any predicted ATU is named a no 5'-end gene. We identified 2,177/2,005 5'-end genes and 1,266/1,160 no 5'-end genes of the predicted ATUs for M9Enrich_Seq/RiEnich. A gene validated by experimental TSSs or TF binding sites means that it is the immediate downstream gene of an experimental TSS or TF binding site. As a result, the proportion of 5'-end genes of the predicted ATUs that were validated by experimental TSSs or TF binding sites was over 1.7 times greater than that of the no 5'-end genes (Table 1). Specifically, the proportion of 5'-end genes (29%/30% for M9Enrich_Seq/RiEnrich_Seq) validated by experimental TF binding sites was over three times greater than the no 5'-end genes (9.2%/9.0% for M9Enrich_Seq/RiEnrich_Seq). These results further verified the reliability of the ATUs predicted by SeqATU in terms of the TSS level. In addition, four other experimental TSS or promoter datasets from RegulonDB (*19*), dRNA-seq (*14*), and Cappable-seq (*13*) were also examined. The results are shown in table S3, and we also found a higher proportion of 5'-end genes of the predicted ATUs validated by experimental TSSs or promoters than that of no 5'-end genes.

We also used two experimental TTS datasets of *E. coli* from SEnd-seq (*7*) and RegulonDB (*19*) to

verify the reliability of predicted ATUs by SeqATU in terms of TTS level. These two experimental TTS datasets were named dataset 3 and dataset 4, respectively. There were 1,540 experimental TTSs in dataset 3 and 367 experimental TTSs in dataset 4. We considered the 3'-end genes and no 3'-end genes of the predicted ATUs by SeqATU. A gene that is not the 3'-end gene of any predicted ATU is named a no 3'-end gene. We identified 2,290/2,187 3'-end genes and 1,153/978 no 3'-end genes of the predicted ATUs for M9Enrich_Seq/RiEnrich_Seq. A gene validated by experimental TTSs means that it is the immediate upstream gene of an experimental TTS. As a result, the proportion of 3'-end genes of the predicted ATUs that were validated by experimental TTSs was over two times greater than that of no 3'-end genes (Table 2). Specifically, the proportion of 3'-end genes (51%/53% for M9Enrich_Seq/RiEnrich_Seq) validated by experimental TTSs from SEnd-seq was over three times greater than that of no 3'-end genes (15%/14% for M9Enrich_Seq/RiEnrich_Seq). These results further verified the reliability of the ATUs predicted by SeqATU in terms of the TTS level. In addition, two other computationally predicted TTS datasets from the works by Nadiras *et al*. (*40*) and Kingsford *et al*. (*41*) were also examined. The results are shown in table S4, and we also found the proportion of 3'-end genes (63%/62% for M9Enrich_Seq/RiEnrich_Seq) validated by computationally predicted Rho-independent TTSs was over two times greater than that of no 3'-end genes (29%/29% for M9Enrich_Seq/RiEnrich_Seq).

Please place Table 1 here.

Please place Table 2 here.

The gene pairs frequently encoded in the same ATUs are more functionally related than those that can belong to two distinct ATUs

Functional analysis was conducted by integrating GO terms from the Gene Ontology (GO) database (*42*). In detail, we measured the level of functional relatedness for two types of consecutive gene pairs, which is similar to the definition in the work by Mao *et al*. (*38*). Two types of consecutive gene pairs were (*i*) gene pairs each consisting of a 5'-end gene of an ATU and the gene in its immediate upstream on the same strand and (*ii*) all the other gene pairs inside an ATU (Fig. 7A). In addition, we used a scoring scheme to measure the GO-based functional similarity between a pair of genes by Wu *et al*. (*43*). This study developed a GO similarity score and showed that the larger the score, the more likely that two genes are functionally related. In brief, the GO similarity score of a gene pair g_k and g_j is denoted as $S_{GO}(g_k, g_j)$:

$$S_{GO}(g_k, g_j) = max_{V_k \in V(g_k),\ V_j \in V(g_j)}\ s(V_k, V_j)$$

where V_k and V_j are the GO terms assigned to g_k and g_j, respectively; $s(V_k, V_j)$ is the maximal number of common terms between paths in the two GO graphs induced by the GO terms V_k and V_j.

As a result, the mean GO similarity score was higher for type-*ii* gene pairs (5.97 *versus* 4.04 for M9Enrich_Seq and 5.86 *versus* 3.91 for RiEnrich_Seq) than for type-*i* gene pairs. A total of 574/524 type-*ii* gene pairs had GO similarity scores greater than four (64%/63% of a total of 899/834), while only 461/404 type-*i* gene pairs had GO similarity scores greater than four (36%/34% of a total of 1,274/1,179) for M9Enrich_Seq/RiEnrich_Seq. We also applied a χ^2-test (*44*) to determine whether the

371 distribution of $S_{GO}(g_k, g_j)$ was different for the type-*i* gene pairs and type-*ii* gene pairs. The χ^2-
372 statistics corresponded to a *P*-value less than 10^{-4}, which revealed that the distribution of $S_{GO}(g_k, g_j)$
373 for the type-*ii* gene pairs was significantly different from the type-*i* gene pairs. Fig. 7B shows the
374 distribution of $S_{GO}(g_k, g_j)$ for the type-*i* gene pairs and the type-*ii* gene pairs. These results strongly
375 indicated that the type-*ii* gene pairs had a higher degree of GO similarity than the type-*i* gene pairs,
376 suggesting that the gene pairs frequently encoded in the same ATUs (type-*ii* gene pairs) are more
377 functionally related than those that can belong to two distinct ATUs (type-*i* gene pairs).

378 We also carried out a similar analysis of the two different gene pairs based on KEGG enrichment
379 analysis (see more details in method S9) and found that the proportion of type-*ii* gene pairs (59%/57%
380 for M9Enrich_Seq/RiEnrich_Seq), whose two genes were contained in the same KEGG pathway, was
381 higher than the proportion of type-*i* gene pairs (32%/28% for M9Enrich_Seq/RiEnrich_Seq) (Fig. 7C).
382 The distribution of the KEGG similarity scores of the two different types of gene pairs is shown in Fig.
383 7D, suggesting that genes of type-*ii* gene pairs have a higher probability of participating in the same
384 KEGG pathway than those of type-*i* gene pairs.

385 Please place Fig. 7 here.

386 **DISCUSSION**

387 We developed SeqATU, the first computational method for genome-scale ATU prediction by analyzing
388 next- and third-generation RNA-Seq data, using a CQP model. Linear constraints provided by the bias

rate of read distribution were, for the first time, integrated into the CQP model. Positional bias refers to the non-uniform distribution of reads over different positions of a transcript (*33, 35*), which is handled by learning non-uniform read distributions from given RNA-Seq reads (*32*) or modeling the RNA degradation (*45*). The bias rate function we proposed can address the non-uniform read distribution along mRNA transcripts and also be desirable for standard next-generation RNA-Seq data that involves more degraded mRNAs, as the exponential function has been used to model the degradation of mRNA transcripts (*45*). As a result, a total of 2,973 distinct ATUs for M9Enrich_Seq and 2,767 distinct ATUs for RiEnrich_Seq were identified by SeqATU. The precision and recall reached 0.67/0.64 and 0.67/0.68, respectively, based on perfect matching and 0.77/0.74 and 0.75/0.76, respectively, based on relaxed matching for M9Enrich_Seq/RiEnrich_Seq. We further validated predicted ATUs using experimental transcription factor binding sites or transcription termination sites from RegulonDB and SEnd-Seq. In addition, the proportion of the 5'- or 3'-end genes of predicted ATUs that were validated by experimental transcription factor binding sites and transcription termination sites was over three times greater than that of no 5'- or 3'-end genes, demonstrating the high reliability of predicted ATUs. Gene pairs frequently encoded in the same ATUs were more functionally related than those that can belong to two distinct ATUs according to GO and KEGG enrichment analyses. These results demonstrated the reliability and accuracy of our predicted ATUs, implying the ability of SeqATU to reveal the transcriptional architecture of the bacterial genome.

In fact, the ATU architecture of bacteria is much more complex than that determined with currently

used experimental techniques. We investigated the 5'-end genes and no 5'-end genes of the experimental ATUs identified by SMRT-Cappable-seq (*6*) using a combination of experimental TSSs from RegulonDB (*19*), dRNA-seq (*14*), Cappable-seq (*13*), and SEnd-seq (*7*). As a result, we found that the proportion of 5'-end genes (99%) validated by experimental TSSs was not significantly different from that of no 5'-end genes (92%). The high percentage of no 5'-end genes validated by experimental TSSs implied that the ATUs identified by experimental techniques are only a small proportion of the comprehensive ATUs in bacterial organisms due to the dynamic mechanisms of ATUs. These results further verified the necessity of developing robust computational methods for ATU identification.

SeqATU not only provides a powerful tool to understand the transcription mechanism of bacteria but also provides a fundamental tool to guide the reconstruction of a genome-scale transcriptional regulatory network. First, the ATU structure can help us to make new functional predictions, as genes in an ATU tend to have related functions. Second, ATUs can elucidate condition-specific uses of alternative sigma factors (*8, 46*). For example, the *thrLABC* operon is regulated by transcriptional attenuation. Totsuka *et al*. found that under the log phase growth condition, the *thrLABC* operon is the only transcript, while two transcripts are found under stationary phase growth condition, the *thrLABC* and *thrBC*. As validated experimentally, σ^S can regulate the additional promoter located in front of *thrB* under the stationary phase growth condition and then separately regulate *thrBC*, which elucidates the condition-specific uses of σ^S (*8*). Third, understanding the ATU structure is of great help to construct transcriptional and translation regulatory networks, such as for the construction of the σ-TUG (σ-factor-transcription unit

gene) network (*47*). The transcription regulatory network consists of nodes (ATU and regulatory proteins) and links (interactions) (*48*), and the comprehensive ATU structure can provide a nearly complete set of nodes, which can improve the accuracy of regulatory prediction.

Although SeqATU has obtained satisfactory predicted results, there are still several challenges regarding the computational prediction of ATUs. On the one hand, due to the influence of the 3' untranslated region (UTR) and 5' untranslated region (UTR) in the intergenic regions, the expression value of intergenic regions cannot be reproduced perfectly by the same calculation used for the expression value of genetic regions. Without accurate reproduction, it is difficult to obtain the best expression combination of ATUs by the programming model based on the expression value of genetic and intergenic regions. On the other hand, due to the lack of strand-specific RNA-Seq data, it is difficult to distinguish the expression level of intergenic regions between two consecutive genes on the same strand derived from ATUs containing these two genes or antisense RNAs (asRNAs) (*6, 49*). All of these challenges and the great significance of ATU prediction inspire and encourage us to discover more information to determine the ATU structure in bacteria. For example, we plan to add high confidence TSSs and TTSs information to our programming model in the future. Additionally, since the microbiome is increasingly recognized as a critical component in human diseases, such as inflammatory bowel disease (*50*), antibiotic-associated diarrhoea (*51*), neurological disorders (*52*), and cancer (*53*) (*54*), predicting new ATUs of uncultured species from metagenomic and metatranscriptomic data is of great significance in uncovering new regulatory pathway and metabolic products during the development of

446 diseases (*55*). However, due to a majority of species with unknown genomes or genome annotations
447 within a microbial community, ATU prediction on metagenomics and metatranscriptomics is still a
448 challenging task, which encourage us to pay more attention on it.

449 **REFERENCES**

450 1. F. Jacob, D. Perrin, C. Sanchez, J. Monod, Operon: a group of genes with the expression
451 coordinated by an operator. *C R Hebd. Seances. Acad. Sci* **250**, 1727-1729 (1960).

452 2. F. Jacob, J. Monod, Genetic regulatory mechanisms in the synthesis of proteins. *J. Mol. Biol.* **3**,
453 318-356 (1961).

454 3. Z. Liu, J. Feng, B. Yu, Q. Ma, B. Liu, The functional determinants in the organization of bacterial
455 genomes. *Brief. Bioinform.*, doi.org/10.1093/bib/bbaa1172 (2020).

456 4. W.-C. Chou, Q. Ma, S. Yang, S. Cao, D. M. Klingeman, S. D. Brown, Y. Xu, Analysis of strand-
457 specific RNA-seq data using machine learning reveals the structures of transcription units in
458 Clostridium thermocellum. *Nucleic Acids Res.* **43**, e67-e67 (2015).

459 5. S.-Y. Niu, B. Liu, Q. Ma, W.-C. Chou, rSeqTU—a machine-learning based R package for
460 prediction of bacterial transcription units. *Frontiers in genetics* **10**, 374 (2019).

461 6. B. Yan, M. Boitano, T. A. Clark, L. Ettwiller, SMRT-Cappable-seq reveals complex operon
462 variants in bacteria. *Nat. Commun.* **9**, 3676 (2018).

7. X. Ju, D. Li, S. Liu, Full-length RNA profiling reveals pervasive bidirectional transcription terminators in bacteria. *Nature microbiology* **4**, 1907-1918 (2019).

8. K. Totsuka, K. Totsuka, The Transcription Unit Architecture of the Escherichia Coli Genome. *Nat. Biotechnol.* **27**, 1043-1049 (2009).

9. A. H. Bhat, D. Pathak, A. Rao, The alr-groEL1 operon in Mycobacterium tuberculosis: an interplay of multiple regulatory elements. *Scientific Reports* **7**, 43772 (2017).

10. C. M. Sharma, S. Hoffmann, F. Darfeuille, J. Reignier, S. Findeiß, A. Sittka, S. Chabas, K. Reiche, J. Hackermüller, R. Reinhardt, The primary transcriptome of the major human pathogen Helicobacter pylori. *Nature* **464**, 250-255 (2010).

11. J. M. Durand, G. R. Bjork, Putrescine or a combination of methionine and arginine restores virulence gene expression in a tRNA modification-deficient mutant of Shigella flexneri: a possible role in adaptation of virulence. *Mol. Microbiol.* **47**, 519-527 (2010).

12. L. E. Wroblewski, R. M. Peek, K. T. Wilson, Helicobacter pylori and gastric cancer: factors that modulate disease risk. *Clin. Microbiol. Rev.* **23**, 713-739 (2010).

13. L. Ettwiller, J. Buswell, E. Yigit, I. Schildkraut, A novel enrichment strategy reveals unprecedented number of novel transcription start sites at single base resolution in a model prokaryote and the gut microbiome. *BMC Genomics* **17**, 199-199 (2016).

14. M. K. Thomason, T. Bischler, S. K. Eisenbart, K. U. Forstner, A. Zhang, A. Herbig, K. Nieselt, C. M. Sharma, G. Storz, Global transcriptional start site mapping using differential RNA sequencing reveals novel antisense RNAs in Escherichia coli. *J. Bacteriol.* **197**, 18-28 (2015).

15. T. Bischler, H. S. Tan, K. Nieselt, C. M. Sharma, Differential RNA-seq (dRNA-seq) for annotation of transcriptional start sites and small RNAs in Helicobacter pylori. *Methods* **86**, 89-101 (2015).

16. D. Dar, M. Shamir, J. Mellin, M. Koutero, N. Stern-Ginossar, P. Cossart, R. Sorek, Term-seq reveals abundant ribo-regulation of antibiotics resistance in bacteria. *Science* **352**, 6282 (2016).

17. J. Clauwaert, G. Menschaert, W. Waegeman, An in-depth evaluation of annotated transcription start sites in E. coli using deep learning. *bioRxiv*, doi: https://doi.org/10.1101/2020.03.16.993501, 4 November 2020, pre-print: not peer-reviewed. (2020).

18. S. Goodwin, J. D. Mcpherson, W. R. Mccombie, Coming of age: ten years of next-generation sequencing technologies. *Nat. Rev. Genet.* **17**, 333-351 (2016).

19. A. Santos-Zavaleta, H. Salgado, S. Gama-Castro, M. Sánchez-Pérez, L. Gómez-Romero, D. Ledezma-Tejeida, J. S. García-Sotelo, K. Alquicira-Hernández, L. J. Muñiz-Rascado, P. Peña-Loredo, RegulonDB v 10.5: tackling challenges to unify classic and high throughput knowledge of gene regulation in E. coli K-12. *Nucleic Acids Res.* **47**, D212-D220 (2018).

20. N. Sierro, Y. Makita, M. J. L. De Hoon, K. Nakai, DBTBS: a database of transcriptional regulation in Bacillus subtilis containing upstream intergenic conservation information. *Nucleic Acids Res.*

36, 93-96 (2008).

21. P. S. Dehal, M. P. Joachimiak, M. N. Price, J. T. Bates, J. K. Baumohl, C. Dylan, G. D. Friedland, K. H. Huang, K. Keith, P. S. Novichkov, MicrobesOnline: an integrated portal for comparative and functional genomics. *Nucleic Acids Res.* **38**, D396-D400 (2010).

22. H. Cao, Q. Ma, X. Chen, Y. Xu, DOOR: a prokaryotic operon database for genome analyses and functional inference. *Brief. Bioinform.* **20**, 1568-1577 (2019).

23. X. Mao, Q. Ma, C. Zhou, X. Chen, H. Zhang, J. Yang, F. Mao, W. Lai, Y. Xu, DOOR 2.0: presenting operons and their functions through dynamic and integrated views. *Nucleic Acids Res.* **42**, D654-D659 (2013).

24. K. Chetal, S. C. Janga, OperomeDB: A Database of Condition-Specific Transcription Units in Prokaryotic Genomes. *Biomed Research International* **2015**, 1-10 (2015).

25. J. Yang, X. Chen, A. Mcdermaid, Q. Ma, DMINDA 2.0: integrated and systematic views of regulatory DNA motif identification and analyses. *Bioinformatics* **33**, 2586-2588 (2017).

26. T. Blanca, C. Ricardo, C. E. Martinez-Guerrero, M. Enrique, ProOpDB: Prokaryotic Operon DataBase. *Nucleic Acids Res.* **40**, D627-D631 (2012).

27. R. McClure, D. Balasubramanian, Y. Sun, M. Bobrovskyy, P. Sumby, C. A. Genco, C. K. Vanderpool, B. Tjaden, Computational analysis of bacterial RNA-Seq data. *Nucleic Acids Res.* **41**,

e140-e140 (2013).

28. X. Chen, W. Chou, Q. Ma, Y. Xu, SeqTU: A Web Server for Identification of Bacterial Transcription Units. *Scientific Reports* **7**, 43925 (2017).

29. I. A. Garanina, G. Y. Fisunov, V. M. Govorun, BAC-BROWSER: The Tool for Visualization and Analysis of Prokaryotic Genomes. *Frontiers in Microbiology* **9**, 2827 (2018).

30. B. Taboada, K. Estrada, R. Ciria, E. Merino, Operon-mapper: a web server for precise operon identification in bacterial and archaeal genomes. *Bioinformatics* **34**, 4118-4120 (2018).

31. H. Li, R. Durbin, Fast and accurate short read alignment with Burrows–Wheeler transform. *Bioinformatics* **25**, 1754-1760 (2009).

32. Z. Wu, X. Wang, X. Zhang, Using non-uniform read distribution models to improve isoform expression inference in RNA-Seq. *Bioinformatics* **27**, 502-508 (2011).

33. A. Roberts, C. Trapnell, J. Donaghey, J. L. Rinn, L. Pachter, Improving RNA-Seq expression estimates by correcting for fragment bias. *Genome Biol.* **12**, 1-14 (2011).

34. R. Bohnert, G. Rï¿ ½tsch, rQuant. web: a tool for RNA-Seq-based transcript quantitation. *Nucleic Acids Res.* **38**, W348-W351 (2010).

35. W. Li, T. Jiang, Transcriptome assembly and isoform expression level estimation from biased RNA-Seq reads. *Bioinformatics* **28**, 2914-2921 (2012).

532 36. B. Xiong, Y. Yang, F. R. Fineis, J.-P. Wang, DegNorm: normalization of generalized transcript
533 degradation improves accuracy in RNA-seq analysis. *Genome Biol.* **20**, 75 (2019).

534 37. J. Chaitanya, Degradation of mRNA in Escherichia coli. *IUBMB Life* **54**, 315-321 (2010).

535 38. X. Mao, Q. Ma, B. Liu, X. Chen, H. Zhang, Y. Xu, Revisiting operons: an analysis of the landscape
536 of transcriptional units in E. coli. *BMC Bioinformatics* **16**, 356 (2015).

537 39. B. Marie, K. H. Thilo, F. Thierry, T. Mikael, R. Adriana, V. D. Christian, Metabolic pathways of
538 Pseudomonas aeruginosa involved in competition with respiratory bacterial pathogens. *Frontiers*
539 *in Microbiology* **6**, 321 (2015).

540 40. C. Nadiras, E. Eveno, A. Schwartz, N. Figueroa-Bossi, M. Boudvillain, A multivariate prediction
541 model for Rho-dependent termination of transcription. *Nucleic Acids Res.* **46**, 8245-8260 (2018).

542 41. C. L. Kingsford, K. Ayanbule, S. L. Salzberg, Rapid, accurate, computational discovery of Rho-
543 independent transcription terminators illuminates their relationship to DNA uptake. *Genome Biol.*
544 **8**, R22 (2007).

545 42. M. Ashburner, S. Lewis, On Ontologies for Biologists: The Gene Ontology—Untangling the Web.
546 *Novartis Found. Symp.* **247**, 66-80; discussion 80-63, 84-90, 244-252 (2002).

547 43. H. Wu, Z. Su, F. Mao, V. Olman, Y. Xu, Prediction of functional modules based on comparative
548 genome analysis and Gene Ontology application. *Nucleic Acids Res.* **33**, 2822-2837 (2005).

549 44. S. A. Teukolsky, B. P. Flannery, W. Press, W. Vetterling, Numerical Recipes in C: The Art of
550 Scientific Computing. *Cambridge University Press*, Cambridge (1992).

551 45. L. Wan, X. Yan, T. Chen, F. Sun, Modeling RNA degradation for RNA-Seq with applications.
552 *Biostatistics* **13**, 734-747 (2012).

553 46. C. Yanofsky, Attenuation in the control of expression of bacterial operons. *Nature* **289**, 751 (1981).

554 47. B. K. Cho, D. Kim, E. M. Knight, K. Zengler, B. O. Palsson, Genome-scale reconstruction of the
555 sigma factor network in Escherichia coli : topology and functional states. *BMC Biol.* **12**, 4-4 (2014).

556 48. B.-K. Cho, P. Charusanti, M. J. Herrgård, Microbial regulatory and metabolic networks. *Curr. Opin.*
557 *Biotechnol.* **18**, 360-364 (2007).

558 49. A. Toledo-Arana, O. Dussurget, G. Nikitas, N. Sesto, H. Guet-Revillet, D. Balestrino, E. Loh, J.
559 Gripenland, T. Tiensuu, K. Vaitkevicius, The Listeria transcriptional landscape from saprophytism
560 to virulence. *Nature* **459**, 950-956 (2009).

561 50. B. Yue, X. Luo, Z. Yu, S. Mani, Z. Wang, W. Dou, Inflammatory bowel disease: a potential result
562 from the collusion between gut microbiota and mucosal immune system. *Microorganisms* **7**, 440
563 (2019).

564 51. B. H. Mullish, H. R. Williams, Clostridium difficile infection and antibiotic-associated diarrhoea.
565 *Clin. Med.* **18**, 237 (2018).

52. M. Maguire, G. Maguire, Gut dysbiosis, leaky gut, and intestinal epithelial proliferation in neurological disorders: towards the development of a new therapeutic using amino acids, prebiotics, probiotics, and postbiotics. *Rev. Neurosci.* **30**, 179-201 (2019).

53. S. Vivarelli, R. Salemi, S. Candido, L. Falzone, M. Santagati, S. Stefani, F. Torino, G. L. Banna, G. Tonini, M. Libra, Gut microbiota and cancer: from pathogenesis to therapy. *Cancers* **11**, 38 (2019).

54. G. Cammarota, G. Ianiro, A. Ahern, C. Carbone, A. Temko, M. J. Claesson, A. Gasbarrini, G. Tortora, Gut microbiome, big data and machine learning to promote precision medicine for cancer. *Nature Reviews Gastroenterology & Hepatology* **17**, 635-648 (2020).

55. S. S. A. Zaidi, X. Zhang, Computational operon prediction in whole-genomes and metagenomes. *Briefings in functional genomics* **16**, 181-193 (2017).

ACKNOWLEDGEMENTS

Funding: This work was supported by the National Nature Science Foundation of China (NSFC) [61772313 to B.L., 11931008 to B.L.]; Interdisciplinary Science Innovation Group Project of Shandong University (2019); and the Innovation Method Fund of China [2018IM020200 to B.L.]. The authors would like to thank Yang Li for his assistance in language polishing. **Authors' contributions:** B.L., Q.M. and W.C. conceived the basic idea and designed the overall analyses. Q.W. carried out most of the computational analysis and data interpretation. All the authors wrote the manuscript. **Competing**

584 **interests:** The authors declare that they have no competing interests. **Data and materials availability:**
585 The raw data and source code of SeqATU and a detailed tutorial can be found at
586 https://github.com/OSU-BMBL/SeqATU.

587 **FIGURES AND TABLES**

588 **Table 1. Results of predicted ATUs verified by experimental TSSs or TF binding sites.** Overview of
589 the experimental TSS and TF binding site datasets (dataset 1 and dataset 2) and the proportion of 5'-end
590 genes and no 5'-end genes of the predicted ATUs by SeqATU for M9Enrich_Seq and RiEnrich_Seq, which
591 were validated by experimental TSSs or TF binding sites.

		dataset 1	dataset 2
Source		Ju *et al*. (*7*)	RegulonDB TF binding sites
Technique		SEnd-seq	Collection
TSSs/TF binding sites		5,512	3,220
M9Enrich_Seq	**5'-end genes**	83%	29%
	no 5'-end genes	47%	9.2%
RiEnrich_Seq	**5'-end genes**	89%	30%
	no 5'-end genes	44%	9.0%

592

593

594 **Table 2. Results of predicted ATUs verified by experimental TTSs.** Overview of the experimental
595 TTS datasets (dataset 3 and dataset 4) and the proportion of 3'-end genes and no 3'-end genes of the
596 predicted ATUs by SeqATU for M9Enrich_Seq and RiEnrich_Seq, which were validated by
597 experimental TTSs.

		dataset 3	dataset 4
Source		Ju *et al.* (*7*)	RegulonDB TTSs
Technique		SEnd-seq	Collection
TTSs		1,540	3,67
M9Enrich_Seq	**3'-end genes**	51%	11%
	no 3'-end genes	15%	5.2%
RiEnrich_Seq	**3'-end genes**	53%	11%
	no 3'-end genes	14%	4.8%

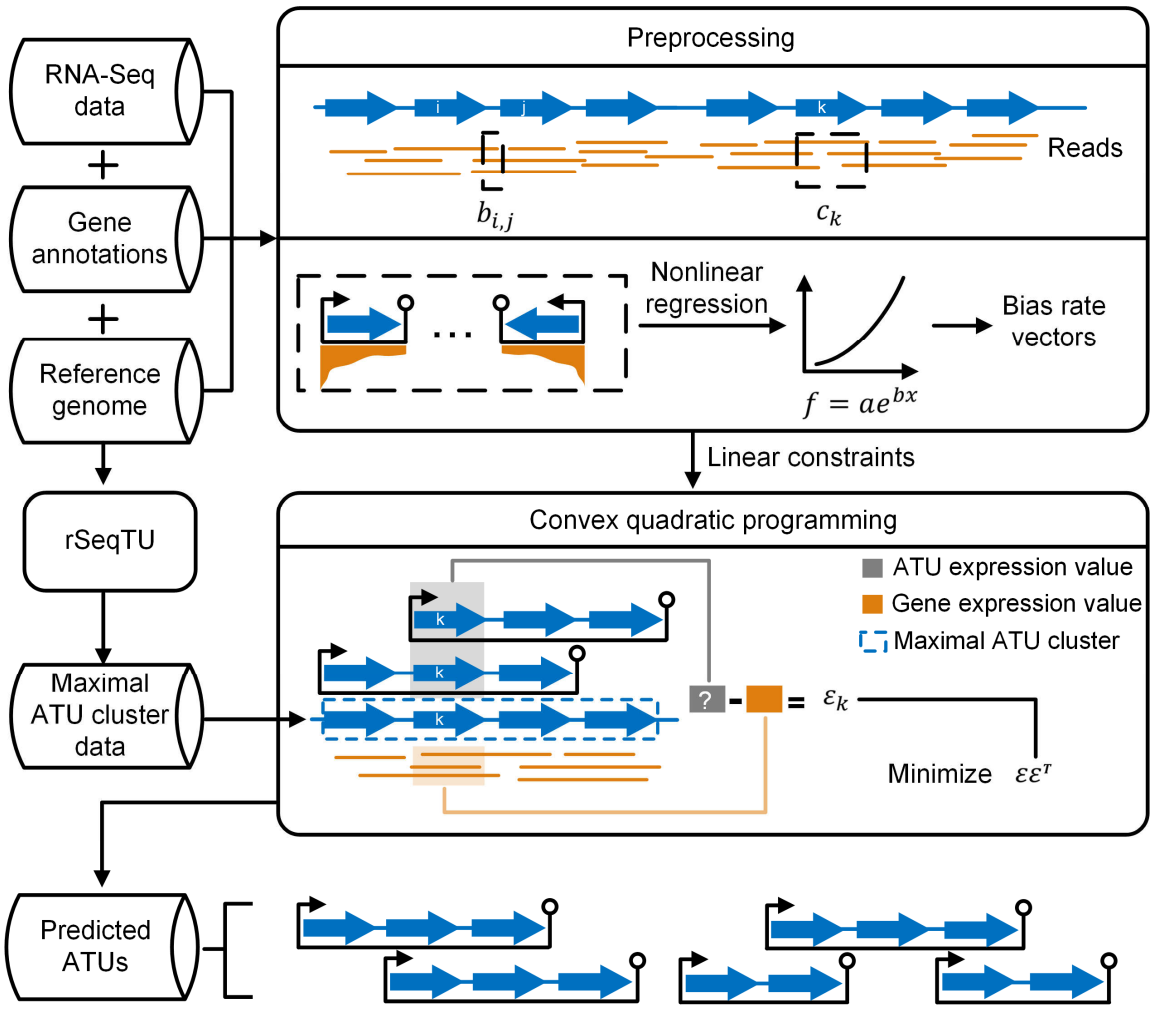

Fig. 1. Schematic overview of SeqATU. The blue arrow and orange line denote gene and RNA-Seq read, respectively. The preprocessing stage requires RNA-Seq data in the FASTQ format, the reference

genome sequence in the FASTA format, and gene annotations in the GFF format, generating linear constraints for the next convex quadratic programming (CQP) stage. There are two steps in the preprocessing stage: (*i*) calculating the expression value of the genetic region c_k and intergenic region $b_{i,j}$ and (*ii*) modelling non-uniform read distribution along mRNA transcripts; specifically, we acquired a bias rate function $f(x) = ae^x$ using nonlinear regression and then constructed genetic or intergenic region bias rate vectors. The maximal ATU cluster data determined by rSeqTU and the linear constraints from preprocessing are both taken as inputs of CQP. CQP seeks the optimum expression combination of all of the to-be-identified ATUs to minimize the gap $\varepsilon\varepsilon^T$ between the predicted ATU expression profile and the genetic and intergenic region expression profile. Finally, the output of CQP is the predicted ATUs.

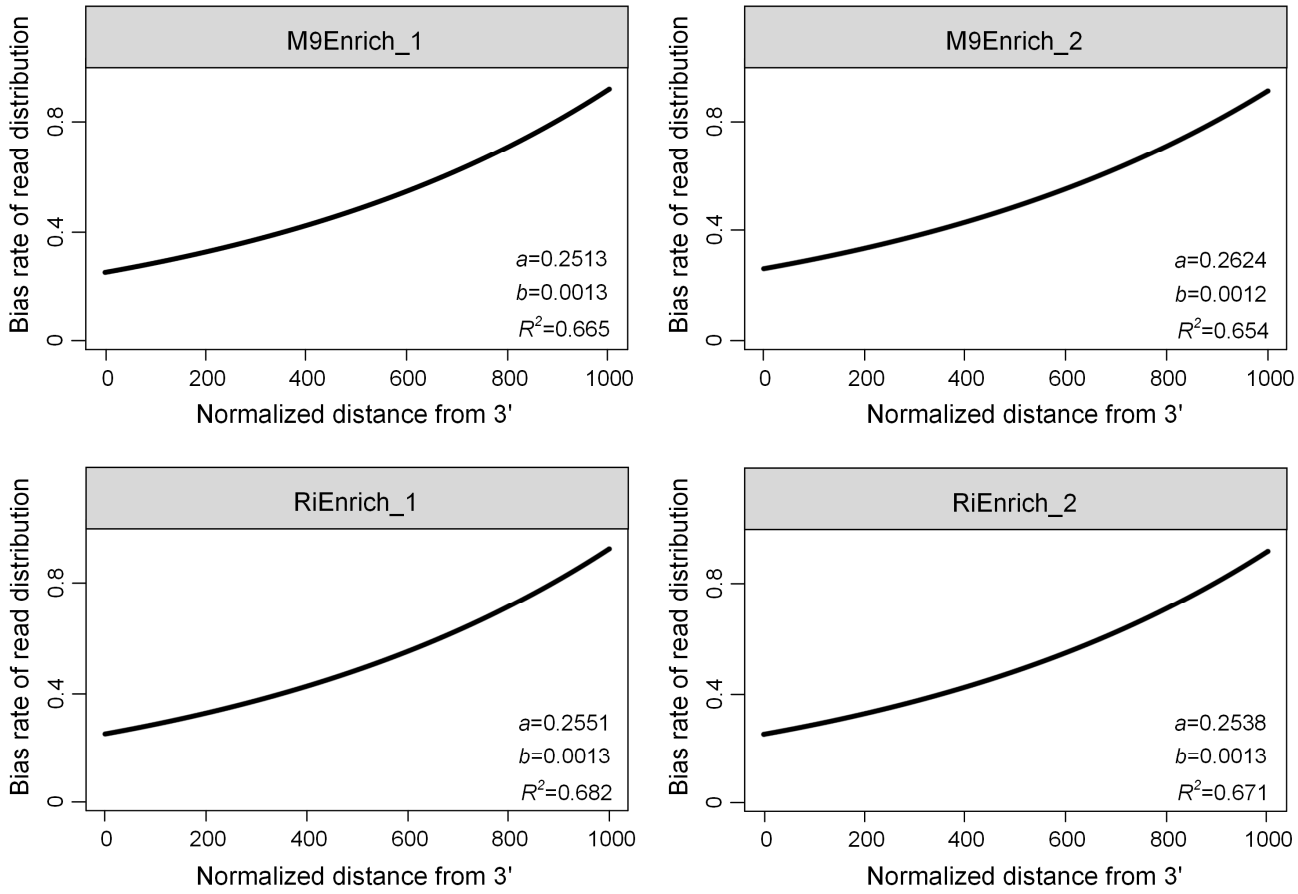

Fig. 2. Results of modelling non-uniform read distribution along mRNA transcripts. The four bias rate functions ($y = ae^{bx}$) by nonlinear regression had similar coefficients (a and b) across the four datasets M9Enrich_1, M9Enrich_2, RiEnrich_1 and RiEnrich_2.

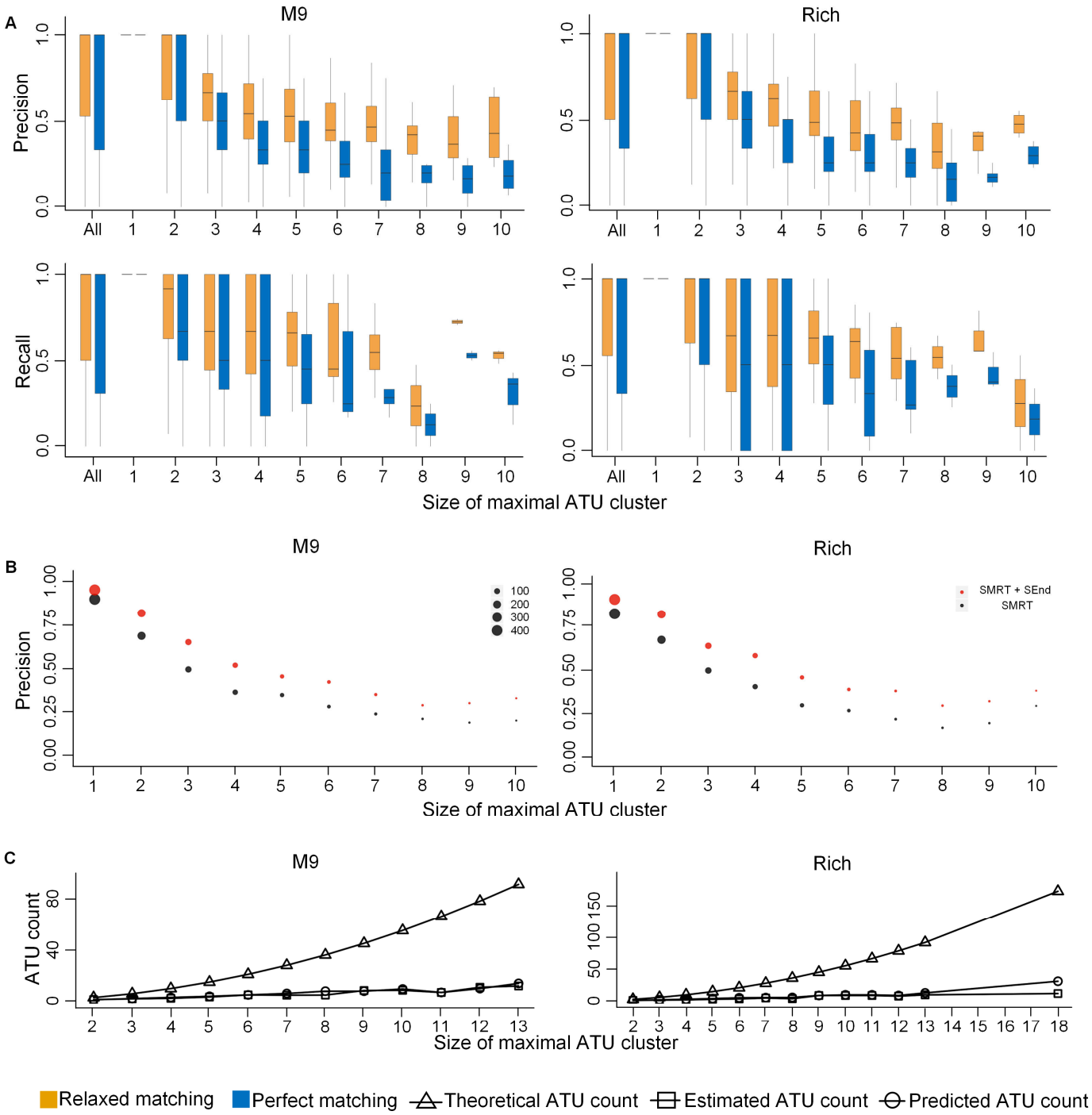

617

618 **Fig. 3. Overall evaluation results of SeqATU.** (**A**) Precision and recall based on perfect matching and

619 relaxed matching for M9Enrich_Seq (left) and RiEnrich_Seq (right) using evaluated ATUs from SMRT-

620 Cappable-seq. (**B**) Average precision based on perfect matching for M9Enrich_Seq (left) and
621 RiEnrich_Seq (right) using evaluated ATUs from SMRT-Cappable-seq (black) and evaluated ATUs from
622 SMRT-Cappable-seq and SEnd-seq (red). The magnitude of the point denotes the number of maximal
623 ATU clusters with same size. (**C**) Average number of ATUs across different sizes of SMRT maximal
624 ATU clusters for M9Enrich_Seq (left) and RiEnrich_Seq (right).

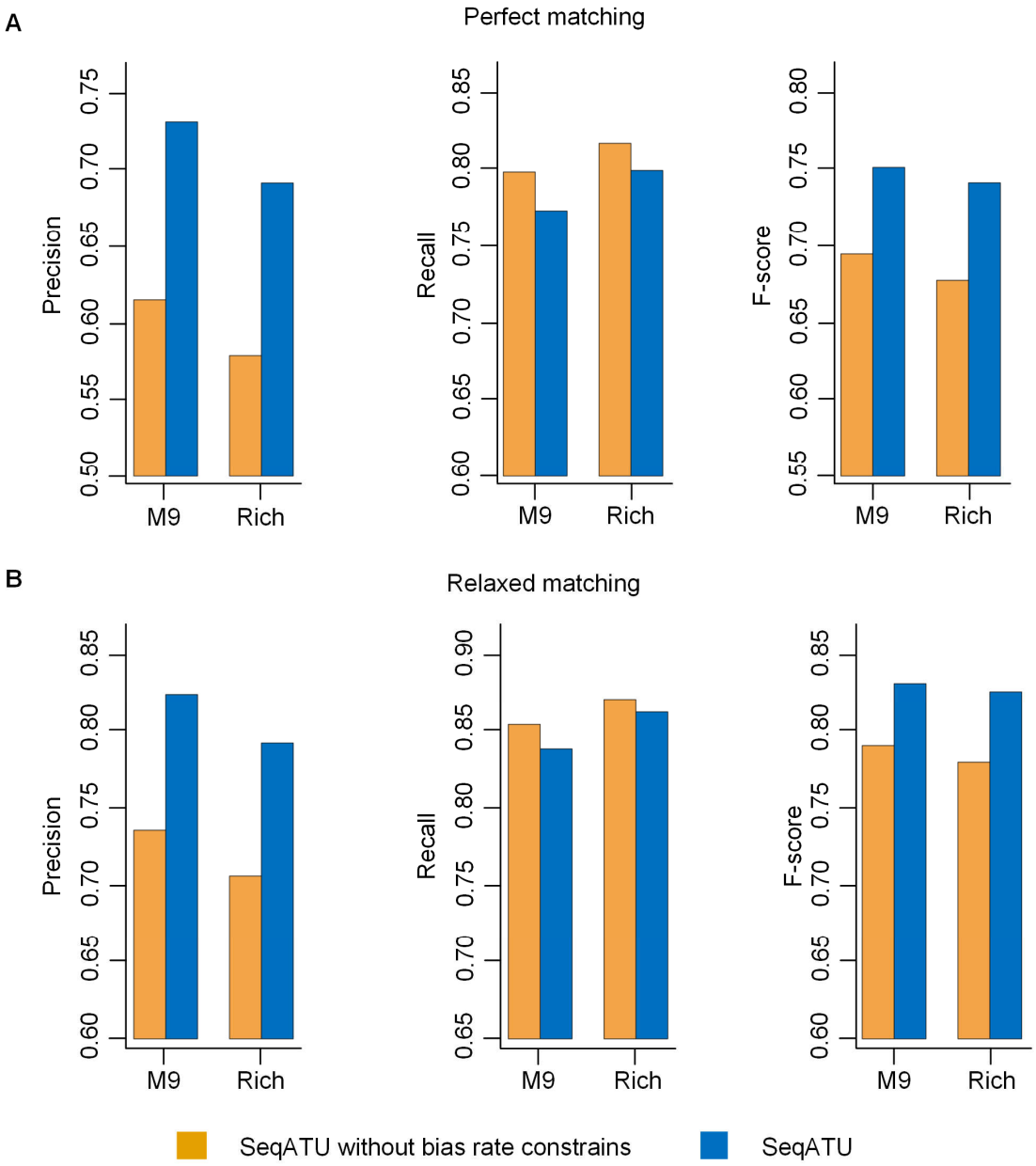

Fig. 4. Comparative analysis of the performance between SeqATU and SeqATU without the bias rate constrains for SMRT maximal ATU clusters. (**A**) Precision, recall and F-score based on perfect matching for M9Enrich_Seq and RiEnrich_Seq. (**B**) Precision, recall and F-score based on relaxed matching for M9Enrich_Seq and RiEnrich_Seq.

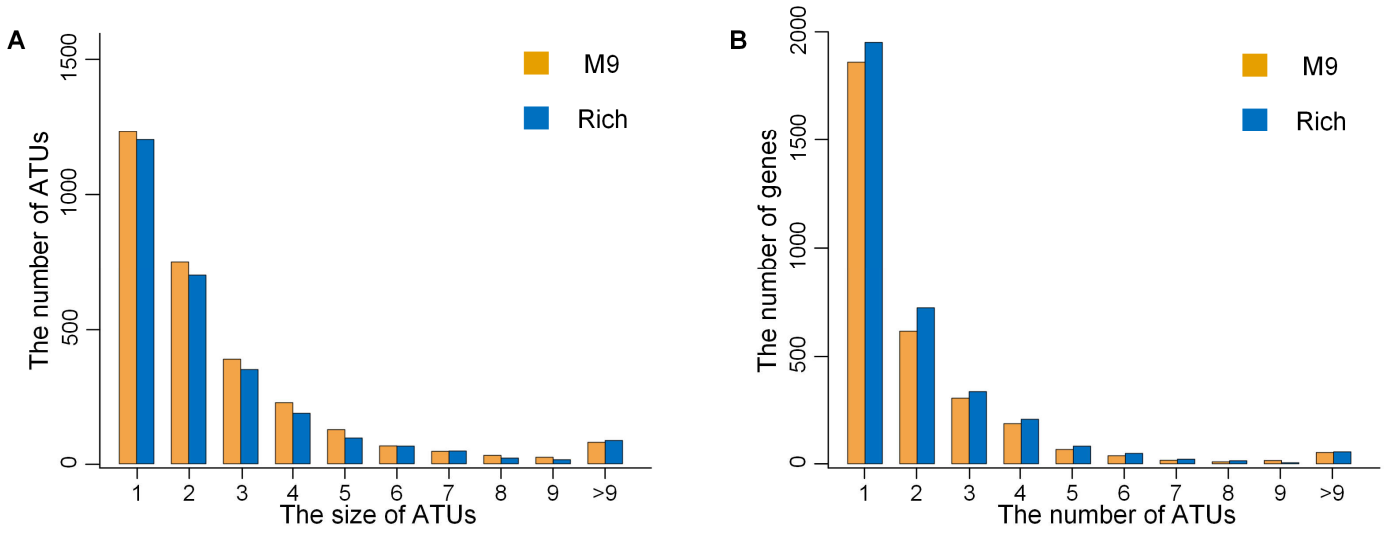

630

631 **Fig. 5. Comprehensive analysis of the predicted ATUs by SeqATU.** (**A**) Number of ATUs across

632 different sizes. The size of an ATU is the number of its component genes. (**B**) Distribution of the number

633 of ATUs per gene.

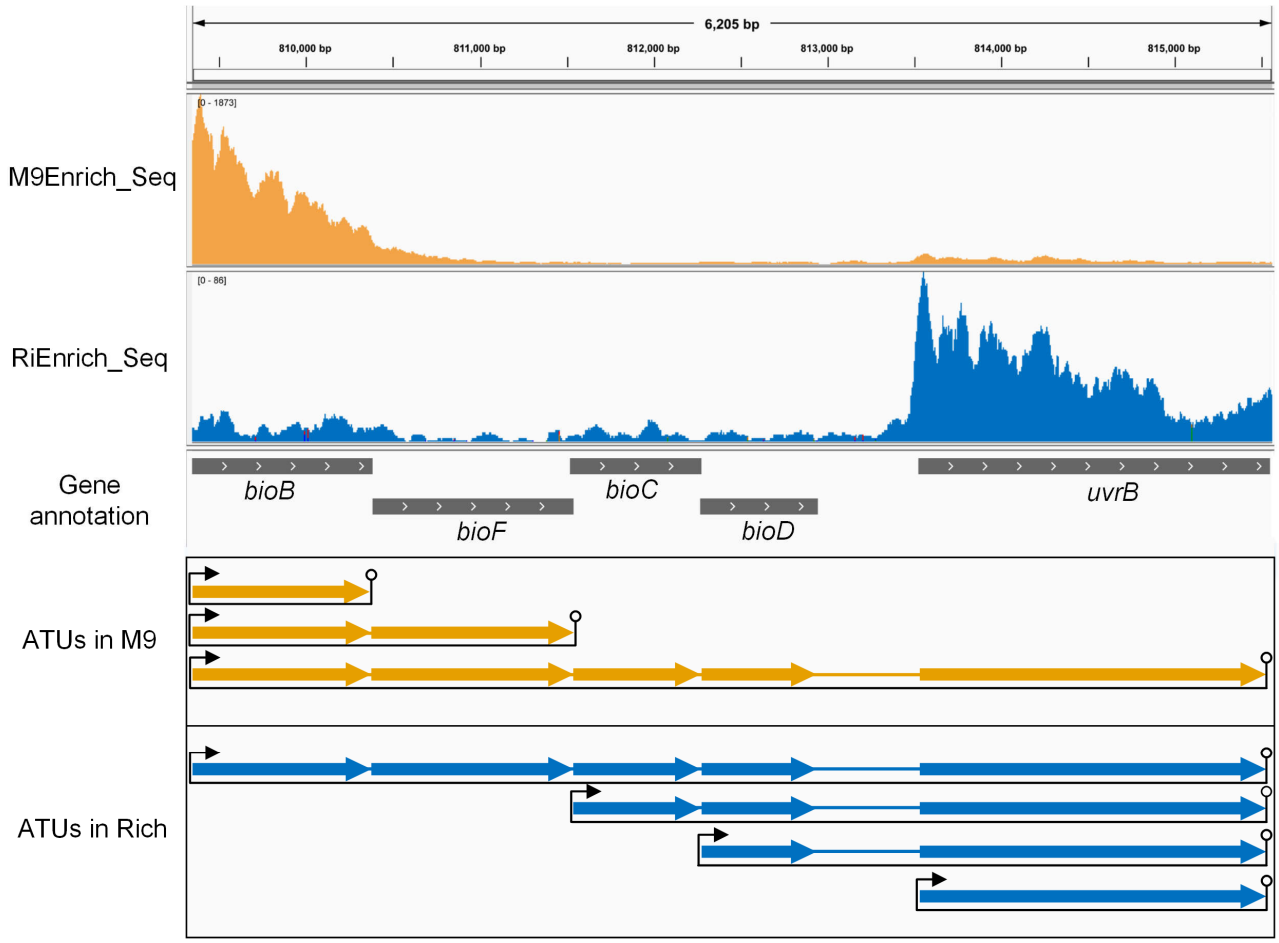

Fig. 6. Integrative Genomics Viewer (IGV) representation of the mapping and ATUs. Mapping and ATUs of M9Enrich_Seq (orange) and RiEnrich_Seq (blue) were shown for the maximal ATU cluster containing the *bioB*, *bioF*, *bioC*, *bioD* and *uvrB* genes.

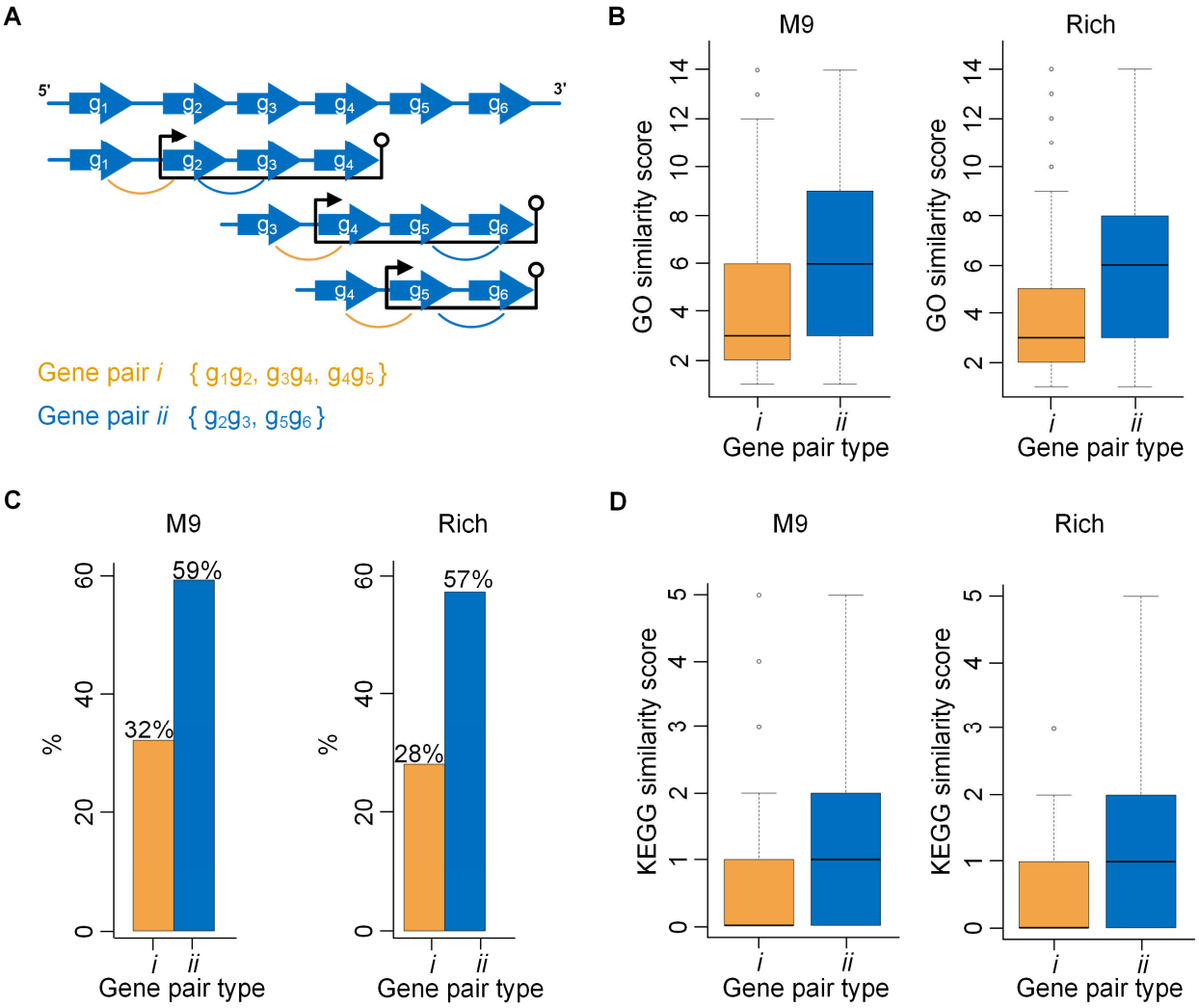

Fig. 7. Interpretation and results of the functional relatedness of different gene pairs based on GO and KEGG enrichment analyses. (**A**) Illustration of two different gene pairs *i* and *ii*. (**B**) Functional relatedness results based on GO enrichment analysis for M9Enrich_Seq (left) and RiEnrich_Seq (right). (**C**) The proportion of two different gene pairs whose genes are contained in the same KEGG pathway for M9Enrich_Seq (left) and RiEnrich_Seq (right). (**D**) The functional relatedness results based on KEGG enrichment analysis for M9Enrich_Seq (left) and RiEnrich_Seq (right).